Scientific Research Publishing

Open Journal of Civil Engineering, 2021, 11, 434-450
https://www.scirp.org/journal/ojce
ISSN Online: 2164-3172
ISSN Print: 2164-3164

Structural Performance of Prefabricated Timber-Concrete Composite Floor Constructed Using Open Web Truss Joist Made of LVL Paraserianthes Falctaria

Ali Awaludin[1*], Urwatul Wusqo[1], Angga Fajar Setiawan[1], Bambang Suhendro[1], Suprapto Siwosukarto[1], Achmad Basuki[1,2], Adrian Leijten[3]

[1]Department of Civil and Environmental Engineering, Universitas Gadjah Mada, Yogyakarta, Indonesia
[2]Department of Civil Engineering, Universitas Sebelas Maret, Surakarta, Indonesia
[3]Faculty of Built Environment, Eindhoven University of Technology, Eindhoven, Netherlands
Email: *ali.awaludin@ugm.ac.id

How to cite this paper: Awaludin, A., Wusqo, U., Setiawan, A.F., Suhendro, B., Siwosukarto, S., Basuki, A. and Leijten, A. (2021) Structural Performance of Prefabricated Timber-Concrete Composite Floor Constructed Using Open Web Truss Joist Made of LVL Paraserianthes Falctaria. *Open Journal of Civil Engineering*, **11**, 434-450.
https://doi.org/10.4236/ojce.2021.114026

Received: September 26, 2021
Accepted: December 27, 2021
Published: December 30, 2021

Abstract

This paper investigates an open web truss joist (OWTJ) made of laminated veneer lumber (LVL) *Paraserianthes falctaria* as a prefabricated timber-concrete composite floor system. The four-point bending test showed that structural performances of the OWTJ, conventional composite floor (CCF), and prefabricated composite floor (PCF) were similar. Although composite action was not developed as no lateral deformation was observed at the shear connectors, installing a concrete slab above the OWTJ can slightly increase the ductility factor of the composite floor. Furthermore, a finite element model was developed, and the model proved to be suitable for simulating the structural performance of the composite floor.

Keywords

LVL Sengon, Open Web Truss Joist, Pre-Fabricated Timber Floor

1. Introduction

The use of green construction materials has increased along with the trend of green building construction in recent decades. Wood from well-managed forests is the most sustainable construction materials and has been used for various purposes since 2500 BC [1] [2] [3]. Timber has been used as a construction material due to its high strength-to-weight ratio, which is essential for buildings in active seismic zones; better sound and thermal insulation; availability especially

in urban areas; and excellent fire resistance [4]. Some structural elements are made of timber, in the forms of solid-sawn (structural) timber, engineered wood products, or composite cross sections. In addition, a structure that is made of timber has a lower embodied energy than those made of concrete and steel [5].

The timber-concrete composite concept has been widely used in the floor system since many years ago. This concept is based on the composite action of timber in the tension zone and concrete in the compression zone connected through shear connectors. This kind of construction offers several advantages, as it is lighter compared with concrete beams and possesses higher timber durability than timber bridges because the timber joist does not experience any direct contact with rain and wind [6]. Previous research focused mainly on the evaluation of the system performance using different timber products as components, such as glulam [7] [8], solid timber [9], laminated veneer lumber (LVL) [10], [11] [12], cross-laminated timber (CLT) [13], and built-up joists. To connect the timber to the concrete part, the following are commonly used: adhesives [8], screws [7] [13] [14], punched metal plates [9], notched connections [10], steel mesh connections [11], or a combination of these connections (hybrid systems) [12]. In about 45% of previous studies, metal dowel-type fastener connections were used [15].

To increase the bending stiffness and reduce the self-weight of the joists, the solid wood joist is replaced with various types of built-up section joists, such as the I-shaped joist [16], box-shaped joist [16], and open web truss joist (OWTJ) (see **Figure 1**). The OWTJ is potentially the most promising regarding the load-bearing capacity compared with other built-up sections. In the OWTJ, the bending and shear forces developed in the floor are transformed into truss action [17]. The use of concrete materials in the timber-concrete composite floor is an innovative way to obtain a structure with a high bearing capacity and stiffness. In addition, to ease the material transportation and construction process, prefabricated elements can be applied in this system. The use of prefabricated elements in the structures is popular since this method provides numerous advantages such as quick and easy installation, low production cost, no-waste materials, and improved quality [18].

Constructing residential buildings with high sustainability is necessary to support sustainable development. However, despite the advancing technology in

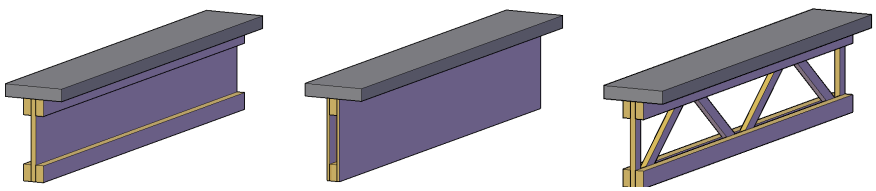

(a) (b) (c)

Figure 1. Timber-concrete composite floors: (a) I-shaped joist; (b) box-shaped joist; (c) OWTJ.

the timber industry, the use of low-strength timber as a construction material to resolve the housing and infrastructure shortage is yet to be implemented [19]. This paper proposes a prefabricated composite floor system made of fast-growing timber that can be applied in low-rise buildings. Laminated veneer lumber produced from the wood species *Paraserianthes falctaria* was used in the OWTJ system and was selected to support the prefabricated concrete slab floor. Both elements were connected by lag screws. The use of *Paraseriathes falctaria* as LVL in this study can encourage and optimize the utilization of local material in industrial sector. The utilization of this composite floor can effectively accelerate the building construction process. There is a need a detail information related to the behavior of the proposed composite floor. Therefore, the structural performance of the proposed composite floor was examined through a four-point bending test. For future applications and development, a numerical analysis was performed to obtain an appropriate composite floor model. The application of the gamma (γ) method to design the OWTJ and concrete composite floor was also evaluated since it is the main method for designing a timber-concrete composite floor.

2. Materials and Methods

2.1. Materials

The wood species *Paraserianthes falctaria*, known as Sengon timber in Indonesia, comes from is a fast-growing tree widely spread in Indonesia that is generally harvested within 5 - 7 years of planting [20]. LVL produced from *Paraserianthes falctaria* has better mechanical properties compared with the solid *Paraserianthes falctaria* wood, as summarized in **Table 1**. This LVL product was made from 2 to 3 mm-thick veneers, glued together using a urea-formaldehyde adhesive, and compressed at 0.6 - 0.7 MPa and a temperature of 105˚C - 110˚C. This LVL product has a great potential to be used as structural materials in shear walls, floor systems, and OWTJs [21].

The LVL *Paraserianthes falctaria* was cut into a certain dimension and arranged to form an OWTJ system, as shown in **Figure 2**. Each truss node was glued using adhesive and compressed with a pressure of 3.5 MPa for 45 minutes.

Table 1. Mechanical properties of LVL *Paraserianthes falctaria* [21].

Mechanical properties	
Density (g/cm^3)	0.41
Modulus of elasticity (N/mm^2)	5700 - 9000
Modulus of rupture (N/mm^2)	39 - 40.57
Compression // (N/mm^2)	4.03
Compression $\perp$ (N/mm^2)	5.40
Tension // (N/mm^2)	46.69

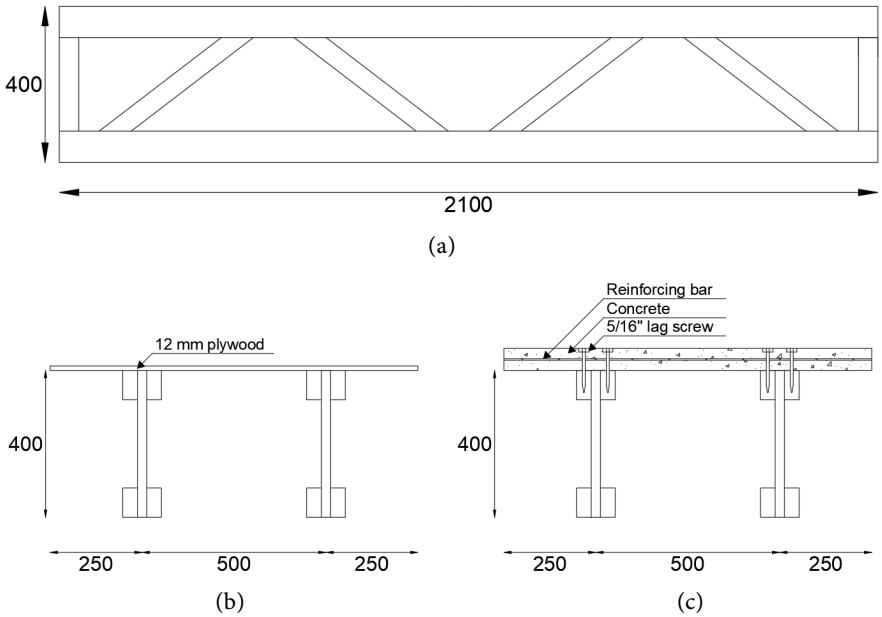

Figure 2. A cross section of (a) an OWTJ, (b) a specimen for TJS, and (c) specimens for CCF and PCF (unit in mm).

Three kinds of produced specimens were tested in this research, denoted as timber joist (TJS), conventional composite floor (CCF), and prefabricated composite floor (PCF). The length of the OWTJ was limited to 2100 mm due to the testing facility limitation. The bearing capacities of these specimens were examined through a four-point bending test.

As shown in **Figure 2**, the specimens for TJS consisted of two OWTJs, to resist the load, while the test specimens for CCF and PCF consisted of two OWTJs and a 60 mm-thick concrete slab with a design compressive strength of 15 MPa at the top. The concrete slab and OWTJ were connected using 5"-5/16 lag screw with a bending yield strength (Fyb) of 568 MPa, as performed in a previous study [22]. The lag screws were inserted perpendicular to the LVL grain. For the PCF specimens, the concrete slab was connected to the OWTJ after 28 days of curing. Lead-holes of 10 mm in diameter were made, and the lag screw was fastened through these holes. To fill the gap between the screw and the hole, the epoxy resin Sikadur 52ID was injected after the lag screws installation.

2.2. Test Setup

The composite floor was examined in a four-point bending test, as presented in **Figure 3**. The load was applied using a 100 kN hydraulic jack. The load was distributed using steel beams located above the composite floor. Three linear variable displacement transducers (LVDTs), one at mid-span and the other two at loading points set at 550 mm from the supports, measured the vertical displacement during the test. The interlayer slips between the concrete slab and OWTJ were also measured using LVDT 4. Each LVDT had a measurement length of up to 50 mm with an accuracy of 0.01 mm.

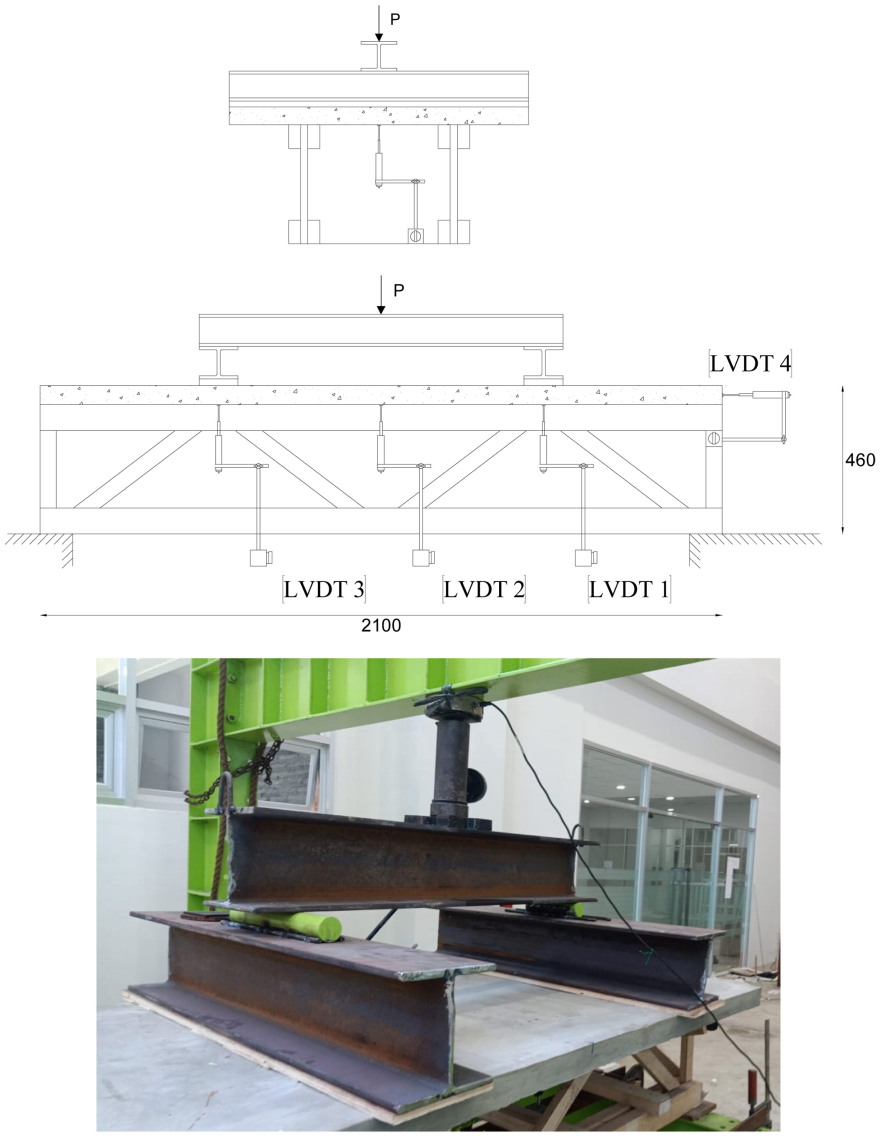

Figure 3. Four-point bending test setup.

2.3. Numerical Analysis

2.3.1. Gamma Method

The gamma (γ) method is a design method that is commonly used to analyze structures with multiple contributing elements. This method is used to calculate the bearing capacity of a timber-concrete composite floor connected by a mechanical fastener. This method is based on the linear elastic theory [23]. The effective bending stiffness of the composite floor, EI_{ef} can be determined using Equation (1).

$$EI_{ef} = \sum_{i=1}^{n}\left(E_i I_i + \gamma_i E_i A_i a_i^2\right) \tag{1}$$

where i refers to the number of elements in the composite floor, E is the modulus of elasticity (MOE), A is the cross-sectional area, and a is the distance from the center of each layer to the center of the composite section. In Equation (1),

the composite action is represented by γ, which can be calculated using Equation (2).

$$\gamma_i = \left[1 + \frac{\pi^2 E_i A_i S_i}{K_i l^2}\right]^{-1} \tag{2}$$

In Equation (2), s is the shear connector spacing, and l is the length of the joist. The lateral shear connector stiffness, K, between the LVL of *Paraserianthes falctaria* and the concrete varied from 2.03 kN/mm to 6.30 kN/mm depending on the concrete compressive strength, penetration depth, and the insertion angle of the lag screw axis [24].

2.3.2. Finite Element Model

In the finite element method, especially in the nonlinear analysis, the method of weighted residual is often used. It is an approximate technique for solving boundary value problems that utilizes trial functions to satisfy the existing boundary conditions [25]. In this research, ABAQUS software was selected to predict the structural performance of the composite floor due to its easiness in defining the behavior of each material.

Figure 4 shows the finite element model of the composite floor. In ABAQUS, OWTJ, plywood sheet, and concrete slab were assumed as 3D solid elements. Connector elements were used to represent the lag screws, in order to connect OWTJ with plywood sheeting or a concrete slab. The stiffness values used for the connectors were obtained from previous studies [24]; the behavior could be classified as linear elastic. The load-controlled four-point bending test was performed applying the load in the specific surface area located 700 mm away from the support.

LVL of Paraserianthes falctaria was modeled as an isotropic material with a density of 4 kN/m^3, MOE of 7083 MPa, and Poisson's ratio of 0.3. Meanwhile, the constitutive equation for concrete shown in **Figure 5** was used. To model the stress-strain behavior of concrete in compression, Mander constitutive model (1988) was used; the stress-strain behavior of concrete in tension was defined as mentioned in Concrete Manual (2015) [26].

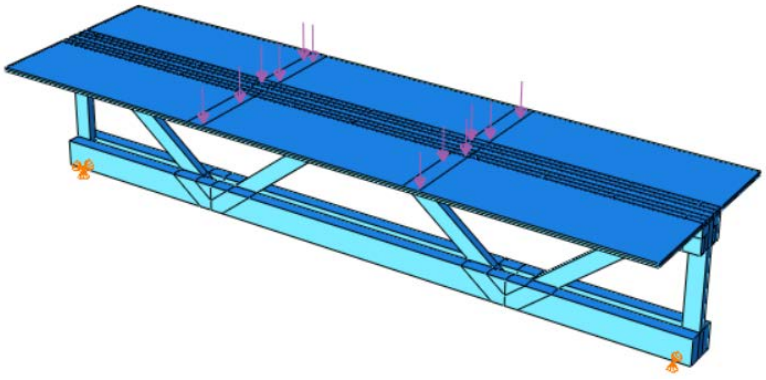

Figure 4. Finite element model of TJS specimen.

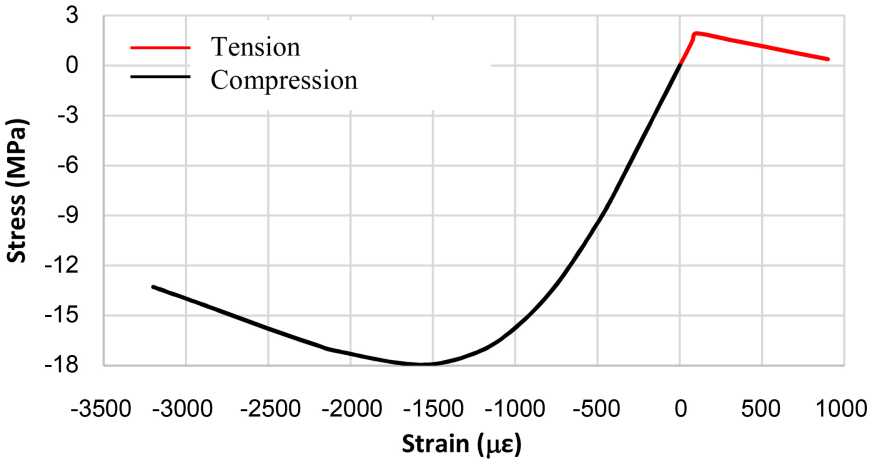

Figure 5. Stress-strain relationship of concrete.

The OWTJ shape was non-prismatic and complex. The tetrahedron mesh (C3D4) type was selected, as shown in **Figure 6**, to obtain a better simulation result. A convergence study was first carried out because the mesh density has a significant influence on both the displacement and stress results [27]. The simulated load-displacement curve given by the FE model was evaluated and compared with the experimental test results for verification. Then, a parametric study was conducted using this verified model to simulate larger spans of similar composite floors.

3. Results and Discussion

3.1. Results

Three concrete compression tests were carried out to evaluate the stress-strain relationship. Three samples were used for this test, with the compression strengths of the concrete cylinders as 17.15 MPa, 22.16 MPa, and 13.72 MPa. Nevertheless, only two stress-strain curves were obtained from these laboratory tests, as shown in **Figure 7**, because the deformation of the first compression test was not properly recorded.

Based on calculation using the γ method, the composite action between concrete and OWTJ was found to be low, only 0.032. Almost no composite action was developed by the construction system. In addition, the maximum load capacity obtained from this method was 69.43 kN. **Figure 8** shows the load-displacement curve of the composite floor obtained from the four-point bending tests. The OWTJ (TJS), composite floor (CCF), and PCF tended to have similar stiffness values and load-bearing capacities. As presented in **Table 2**, the maximum loads that could be supported by the TJS, CCF, and PCF specimens were 47.78 kN, 42.29 kN, and 44.51 kN, respectively. When this maximum load is divided by the area of the floor, the ultimate bearing capacities of TJS, CCF, and PCF are obtained as 22.75 kN/m^2, 20.14 kN/m^2, and 21.19 kN/m^2, respectively. The ultimate bearing strength of TJS was 12.96% and 7.36% higher than

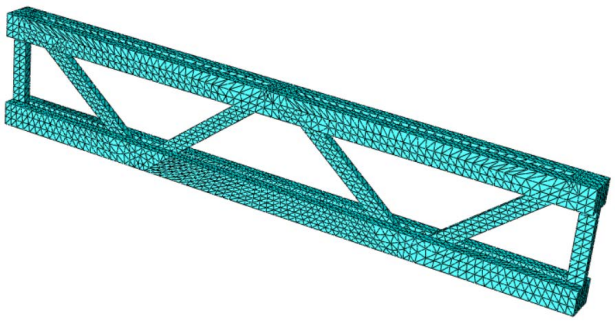

Figure 6. Meshing on OWTJ element.

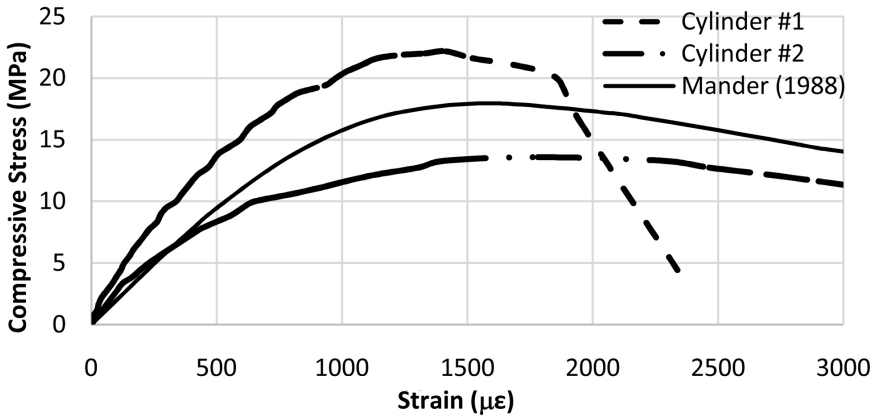

Figure 7. Concrete compression test result.

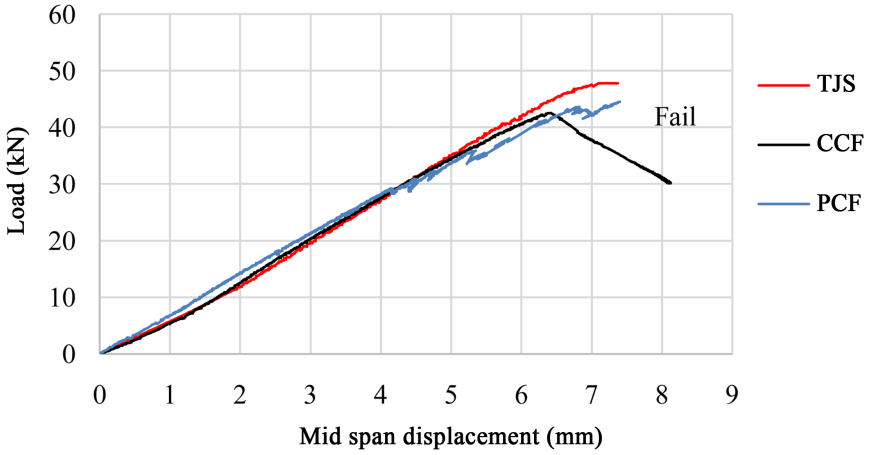

Figure 8. Four-point bending test result of timber-concrete composite floors.

Table 2. Bearing capacities of timber-concrete composite floors.

TJS	CCF	PCF	PCF
Ultimate load (kN)	47.78	42.29	44.51
Ultimate bearing capacity (kN/m^2)	22.75	20.14	21.19
Bearing capacity at service load (kN/m^2)	9.10	8.06	8.48
Load-bearing stiffness (kN/mm)	6.90	7.37	7.30

those of CCF and PCF, respectively. This result is reasonable because the concrete slabs in the CCF and PCF specimens provide the composite floor with an additional self-weight load of 3.18 kN.

The four-point bending test results above show the ultimate bearing capacity of each specimen in the short-term period of loading. Several factors should be considered in determining the capacity of the composite floor at service condition, including creep phenomenon, which may occur during the service life of the structure. Creep is a natural phenomenon in which a structure suffers increasing strain under a constant load. It is very fast in the beginning, then becomes slow, and then stabilizes quickly after a certain period of loading [28]. Stress levels of 25% to 50% of the ultimate load are considered in many creep tests of timber and timber-based composites [29] [30] [31] [32] [33]. According to Schaffer (1982), Boltzmann's superposition principle applies to the stress-strain behavior of a timber structure for stresses up to 40% of the short-term strength [28] [34], where below this stress level, linear stress-strain relation is a good approximation. Therefore, in the current study, the bearing capacity of the proposed composite floor at service load was taken as 40% of the ultimate bearing capacity.

As summarized in **Table 2**, the bearing capacities of TJS, CCF, and PCF at service load were 9.10 kN/m^2, 8.06 kN/m^2, and 8.48 kN/m^2, respectively. These values are quite far from the design load of 1.92 kN/m^2, as stated in SNI 1727:2013—the Minimum Load for Design of Building Structures and Other Structures [35]. Besides the strength requirement, a structure has to meet the serviceability requirement, which is related to the maximum displacement occurring at the service load. Based on the Indonesian Standard SNI 2002, the maximum displacement in the structure at the service load was limited to L/360 [36]. The length of the composite floor was 2100 mm, and this means that the displacement in the composite floor at the serviceability load level must not exceed 5.81 mm. **Figure 8** shows that the maximum mid-span displacements of the TJS, CCF, and PCF at service load were 2.58 mm, 2.55 mm, and 2.50 mm, respectively. The ratios of the bearing capacity at service condition to the minimum design load of TJS, CCF, and PCF were 4.74, 4.20, and 4.41, respectively. The displacements at the service load of TJS and PCF were 56% lower than the displacement limit. Moreover, the displacement at the service load of CCF was 57% lower than the displacement limit. This indicates that the proposed composite floor meets the minimum bearing capacity requirement at the service load, with a sufficient safety factor both in terms of strength and serviceability. However, the bearing capacities at service condition would decrease for a longer span and in the presence of connections in the OWTJ members.

Structure ductility is the ability of a structure to experience large deformation without rupture before failure. This is an important aspect for structures, especially for structures located in seismic zones, as it can be a basis for warning occupants before a structure collapse [37]. The ductility factor was defined by di-

viding the ultimate displacement, Δfailure, by the yield displacement, Δyield, in accordance with the equivalent energy elastic-plastic method [38]. Here, ultimate displacement represents the displacement at failure or at 80% of the peak load. Table 3 summarizes the ductility factor of each specimen.

After reaching the ultimate load capacity, each specimen experienced a different type of failure. As shown in Figure 9, the joint of the TJS specimen failed. The TJS specimen collapsed when the load applied in the structure reached 47.78 kN. The failure of the structure was caused by the glueline shear failure at the node at the top edge and in the middle of the OWTJ.

After the CCF specimen reached its ultimate bearing strength, the diagonal members of OWTJ near the support experienced lateral buckling, resulting in delamination on the LVL member, as shown in Figure 10. In this condition, the capacity of the structure decreased as the displacement increased. The concrete slab did not show damaged when the test was terminated.

Table 3. Ductility factor of composite floor.

Specimen	$\Delta_{failure}$ (mm)	P_{yield} (kN)	Δ_{yield} (mm)	Ductility factor
TJS	7.37	43.22	6.20	1.19
CCF	7.57	34.94	5.05	1.50
PCF	7.40	37.88	5.80	1.28

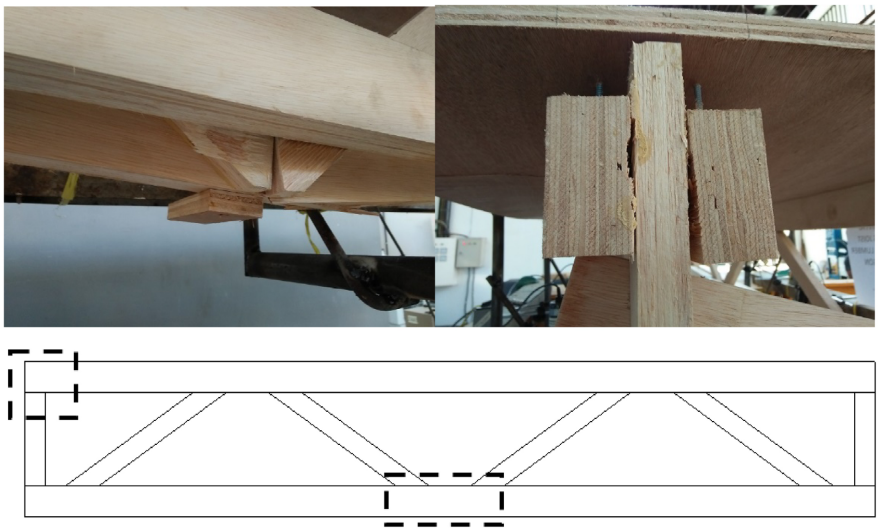

Figure 9. Failure mode of open web truss joist (TJS) specimen.

For the PCF specimen, both the concrete slab and the OWTJ LVL Parasearianthes falctaria showed signs of damage. The failure started with the lateral buckling of one of the diagonal members located near the support, followed by the occurrence of delamination in the LVL member, as shown in Figure 11. In addition, the concrete slab near the shear connector started to show cracks.

The interlayer slip between the concrete slab and upper cord of LVL in the

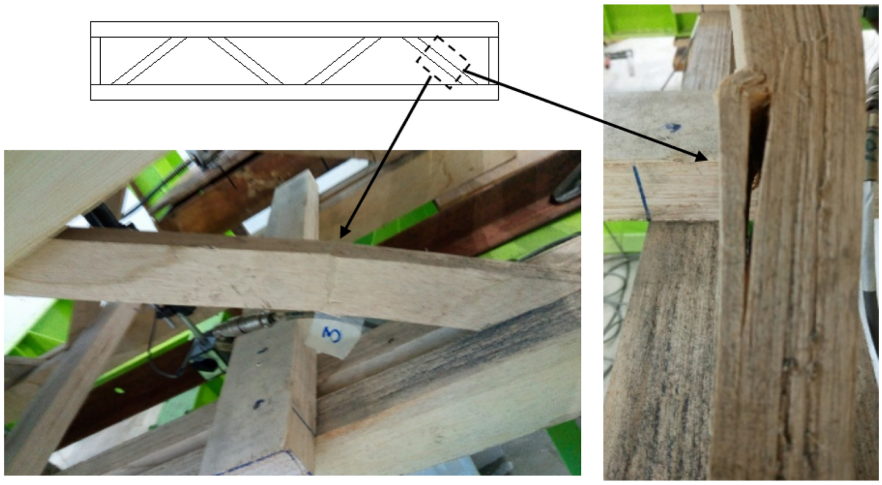

Figure 10. Failure mode of the conventional composite floor (CCF) specimen.

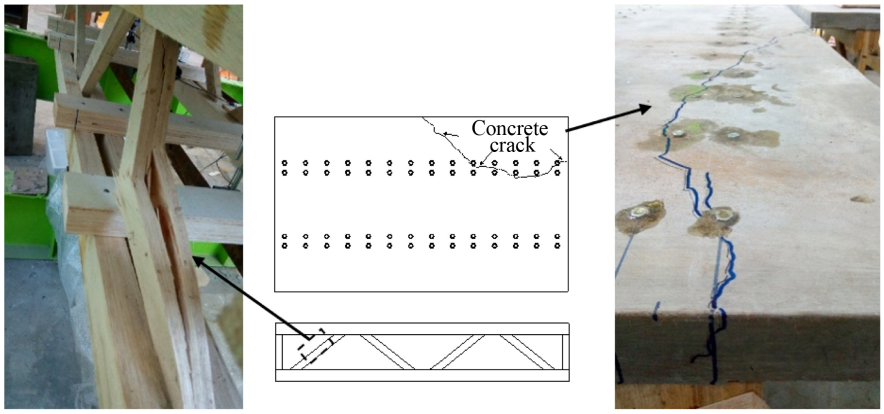

Figure 11. Failure mode of the prefabricated composite floor (PCF) specimen.

OWTJ specimen is shown in Figure 12. Comparing the interlayer slip values between the CCF and PCF specimens, the slips were almost the same at the initial stage of the loading. The epoxy resin that was used to remove the hole clearance the lag screws installation maintained a good bond with the concrete slab. As a result, the structural performance of PCF was similar to that of CCF both in terms of initial stiffness, interlayer slip, and ultimate strength. However, after the load reached 15 kN, the interlayer slip on the PCF specimen became greater than that on the CCF specimen.

In both the CCF and PCF specimens, the concrete slab around the lag screws was removed after the test to observe the shear connector damage. As shown in Figure 13, the lag screw was still straight; no irreversible lateral deformation occurred. This indicates that the shear connector was still in its elastic condition.

3.2. Discussions

3.2.1. The Compatibility of the γ Method with the Composite Floor Structure

As stated earlier, for a built-up timber structure, the γ method can be used to

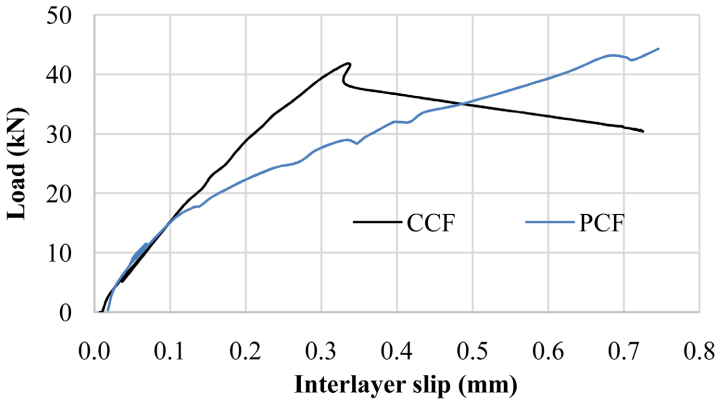

Figure 12. Interlayer slip.

Figure 13. Shear connector after loading test.

predict the degree of composite action, stress distribution along the built-up sections, and the displacement of the structure. However, this method may have some limitations. As shown by the test, the degree of composite action between the concrete and the OWTJ was only 0.032. This small value for the composite action was caused by the large difference in MOE between the concrete and LVL Paraserianthes falctaria. The experimental results also show a similar result, where the load applied in the concrete is distributed directly to the OWTJ, causing damage to the LVL member. The lag screws did not experience any yielding, as evidenced by the very small lateral deformation.

3.2.2. The Pattern of Composite Floor Failure

The experimental result did not provide any specific pattern of composite floor failure. However, one of the diagonal OWTJ members located near the supports of the CCF and PCF specimens experienced buckling failure, followed by delamination in the LVL member; moreover, the concrete near the shear connectors

in the PCF specimens cracked. Predrilling holes in the construction caused some micro-cracks near the holes. This initiated the occurrence of a greater crack in the concrete slab in the PCF specimen, as shown in Figure 11. For further application, predrilling holes in the concrete slab is not recommended. The use of removable steel pipes to create holes during the concreting work is suggested in order to avoid the existence of micro-cracks near the holes.

3.2.3. The Comparison between the Finite Element Model and the Experimental Result

Figure 14 compares the load-displacement curves obtained from the laboratory test and FE model. The displacement was measured at the mid-span, since this location experienced the highest deformation. As shown in Figure 14, the curve of the FE model was close to that of the laboratory test result. This figure also indicates that the introduction of a plywood sheet in the FE model had no significant effect on the FEM result. Therefore, an FEM that only consists of the OWTJ is appropriate for further design and application. Furthermore, for the proposed composite floor, this model is also suitable due to the reasons below.

1) The degree of composite action between the concrete slab and the OWTJ was only 0.032. The concrete slab and OWTJ will not act as a single unit structure but as two separate structural elements.

2) The lag screws did not experience irreversible lateral deformation (see Figure 13). This indicates that there is no high load transfer mechanism in the mechanical joint.

3) Simplifying the concrete slabs as a distributed load acting on the OWTJ will accelerate the simulation process.

A parametric study was conducted to evaluate the structural performance of the OWTJ. Several models for the OWTJ with various span lengths were evaluated using FE simulation. The ultimate capacity of the structure was evaluated to determine two criteria, which are allowable deflection at service load and maximum compression stress in joist members. The capacity of the structure at service condition was then taken as 40% of its ultimate capacity. From Figure 15, it can be concluded that the capacity of the structure will decrease with the

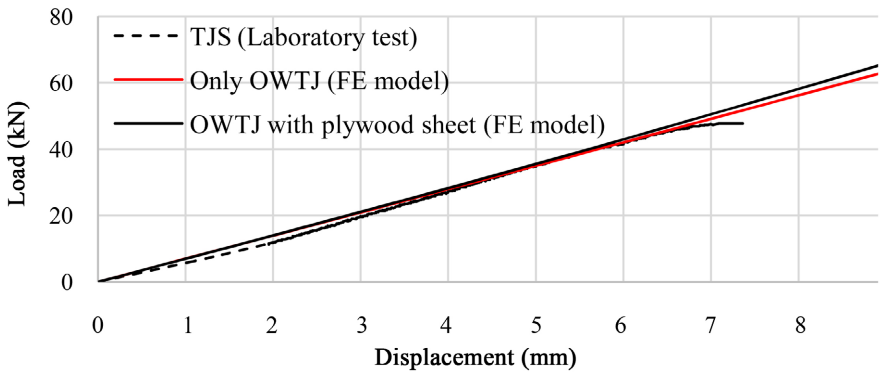

Figure 14. The load-displacement curve of TJS specimen obtained from laboratory test and FE model.

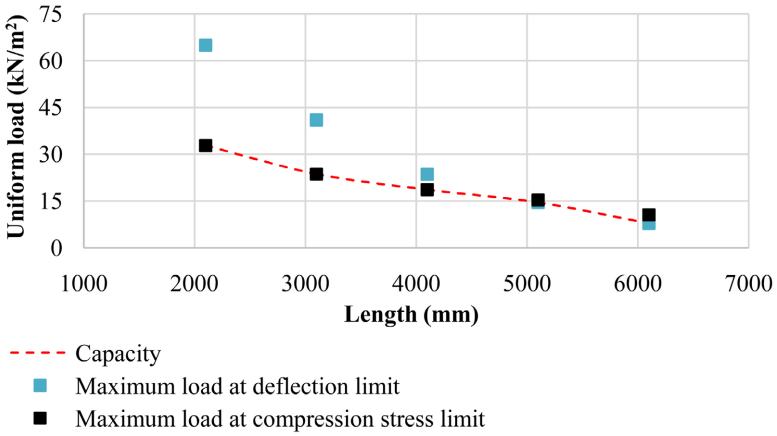

Figure 15. The capacity of OWTJ at service load based on the structure length.

increase of span length. In addition, the capacity of the structure will be governed by the deflection limit of the structure when the span is longer than 5 m.

4. Conclusion

This paper presents a numerical and experimental study on the use of the OWTJ in a composite floor system. The proposed composite floor consists of an OWTJ made of LVL *Paraserianthes falctaria* and a concrete slab connected by lag screws to allow prefabrication. Three specimens, *i.e.*, OWTJ (TJS), CCF, and PCF, were assessed using a four-point bending test. From the experimental work in the laboratory, these three specimens showed similar capacities and structural stiffness values. The composite action between the OWTJ and the concrete slab was extremely small since the difference between the shear connection stiffness and the bending stiffness of the LVL compared with bending stiffness of the concrete (MOE) was not well balanced. After the test, no irreversible lateral deformation was found in the lag screws. Nevertheless, positioning a concrete slab above the OWTJ can increase the ductility factor of the composite floor. From the numerical work, the developed FE model is suitable to simulate the structural performance of the composite floor. The concrete slab above the composite floor can be simplified as a distributed load acting on the OWTJ. For further development, the proposed composite flooring system can be modified by applying different types of connectors and wood materials.

Acknowledgements

The authors gratefully acknowledge the ministry of research and technology of republic Indonesia for the financial support during this research through PTUPT 2019 program. Also, the authors appreciate PT. Sumber Graha Sejahtera for LVL Paraserianthes falctaria material supplies.

Conflicts of Interest

The authors declare no conflicts of interest regarding the publication of this paper.

References

[1] Ramage, M.H., Burridge, H., Busse-Wicher, M., Fereday, G., Reynolds, T., Shah, D.U., Wu, G., Yu, L., Fleming, P., Densley-Tingley, D., Allwood, J., Dupree, P., Linden, P.F. and Scherman, O. (2017) The Wood from the Trees: The Use of Timber in Construction. *Renewable and Sustainable Energy Reviews*, **68**, 333-359. https://doi.org/10.1016/j.rser.2016.09.107

[2] Porteus, J. and Kermani, A. (2007) Structural Timber Design to Eurocode 5. Blackwell Science Ltd., Oxford. https://doi.org/10.1002/9780470697818

[3] Dinwoodie, J.M. (2000) Timber: Its Nature and Behaviour. Taylor & Francis e-Library, New York.

[4] Thelandersson, S. and Larsen, H.J. (2003) Timber Engineering. John Wiley & Sons, West Sussex.

[5] Glover, J., White, D.O. and Langrish, T.A.G. (2002) Wood versus Concrete and Steel in House Construction: A Life Cycle Assessment. *Journal of Forestry*, **100**, 34-41.

[6] Fragiacomo, M., Gregori, A., Xue, J., Demartino, C. and Toso, M. (2018) Timber-Concrete Composite Bridges: Three Case Studies. *Journal of Traffic and Transportation Engineering* (*English Edition*), **5**, 429-438. https://doi.org/10.1016/j.jtte.2018.09.001

[7] Crocetti, R., Sartori, T. and Tomasi, R. (2015) Innovative Timber-Concrete Composite Structures with Prefabricated FRC Slabs. *Journal of Structural Engineering*, **141**, 1-10. https://doi.org/10.1061/(ASCE)ST.1943-541X.0001203

[8] Tannert, T., Endacott, B., Brunner, M. and Vallée, T. (2017) Long-Term Performance of Adhesively Bonded Timber-Concrete Composites. *International Journal of Adhesion and Adhesives*, **72**, 51-61. https://doi.org/10.1016/j.ijadhadh.2016.10.005

[9] Lukaszewska, E. (2009) Development of Prefabricated Timber-Concrete Composite Floors. Luleå University of Technology, Luleå.

[10] Boccadoro, L. and Frangi, A. (2014) Experimental Analysis of the Structural Behavior of Timber-Concrete Composite Slabs Made of Beech-Laminated Veneer Lumber. *Journal of Performance of Constructed Facilities*, **28**, 1-10. https://doi.org/10.1061/(ASCE)CF.1943-5509.0000552

[11] Mudie, J., Sebastian, W.M., Norman, J. and Bond, I.P. (2019) Experimental Study of Moment Sharing in Multi-Joist Timber-Concrete Composite Floors from Zero Load up to Failure. *Construction and Building Materials*, **225**, 956-971. https://doi.org/10.1016/j.conbuildmat.2019.07.137

[12] Tannert, T., Gerber, A. and Vallee, T. (2019) Hybrid Adhesively Bonded Timber-Concrete-Composite Floors. *International Journal of Adhesion and Adhesives*, **97**, Article ID: 102490. https://doi.org/10.1016/j.ijadhadh.2019.102490

[13] Mai, K.Q., Park, A., Nguyen, K.T. and Lee, K. (2018) Full-Scale Static and Dynamic Experiments of Hybrid CLT-Concrete Composite Floor. *Construction and Building Materials*, **170**, 55-65. https://doi.org/10.1016/j.conbuildmat.2018.03.042

[14] Du, H., Hu, X.M., Xie, Z. and Wang, H.C. (2019) Study on Shear Behavior of Inclined Cross Lag Screws for Glulam-Concrete Composite Beams. *Construction and Building Materials*, **224**, 132-143. https://doi.org/10.1016/j.conbuildmat.2019.07.035

[15] Dias, A., Schänzlin, J. and Dietsch, P. (2018) Design of Timber-Concrete Composite Structures. European Cooperation in Science and Technology (COST).

[16] Awaludin, A., Firmanti, A., Muslikh, Theodarmo, H. and Astuti, D. (2017) Wood

Frame Floor Model of LVL *Paraserianthes falcataria*. *Procedia Engineering*, **171**, 113-120. https://doi.org/10.1016/j.proeng.2017.01.317

[17] Yost, J.R., Dinehart, D.W., Gross, S.P., Pote, J.J. and Gargan, B. (2004) Strength and Design of Open Web Steel Joists with Crimped-End Web Members. *Journal of Structural Engineering*, **130**, 2016-2031. https://doi.org/10.1061/(ASCE)0733-9445(2004)130:5(715)

[18] Bachmann, H. and Steinle, A. (2012) Precast Concrete Structures. Ernst & Sohn. https://doi.org/10.1002/9783433600962

[19] Bukauskas, A., Mayencourt, P., Shepherd, P., Sharma, B., Mueller, C., Walker, P. and Bregulla, J. (2019) Whole Timber Construction: A State of the Art Review. *Construction and Building Materials*, **213**, 748-769. https://doi.org/10.1016/j.conbuildmat.2019.03.043

[20] Krisnawati, H., Varis, E., Kallio, M.H. and Kanninen, M. (2011) *Paraserianthes falcataria* (L.) Nielsen: Ecology, Silviculture and Productivity. Center for International Forestry Research (CIFOR). https://doi.org/10.17528/cifor/003394

[21] Awaludin, A., Shahidan, S., Basuki, A., Zuki, S.S.M. and Nazri, F.M. (2018) Laminated Veneer Lumber (LVL) Sengon: An Innovative Sustainable Building Material in Indonesia. *International Journal of Integrated Engineering*, **10**, 17-22.

[22] Wusqo, U., Awaludin, A., Setiawan, A.F. and Irawati, I.S. (2019) Study of Laminated Veneer Lumber (LVL) Sengon to Concrete Joint Using Two-Dimensional Numerical Simulation. *Journal of the Civil Engineering Forum*, **5**, 275-288. https://doi.org/10.22146/jcef.47694

[23] The European Union (2011) Eurocode 5: Design of Timber Structures—Part 1-1: Genera-Common Rules and Rules for Buildings.

[24] Tantisaputri, I.A., Awaludin, A., Siswosukarto, S., Teknik, F. and Mada, U.G. (2019) Analisa Kekuatan Tahanan Lateral Pada Sistem Komposit LVL Kayu Sengon dan Beton Pracetak [Analysis of Lateral Resistant Strength in Composite System LVL Sengon and Concrete]. *Media Komunikasi Teknik Sipil*, **25**, 132-140. https://doi.org/10.14710/mkts.v25i2.23068

[25] Hutton, D.V. (2004) Fundamentals of Finite Element Analysis. McGraw Hill, New York.

[26] ICC (2015) The Strength of Concrete. *Concrete Manual Based on the* 2015 *IBC and ACI* 318-14, International Code Council, Inc., Washington DC, 23-27.

[27] Mesh Convergence. https://abaqus-docs.mit.edu/2017/English/SIMACAEGSARefMap/simagsa-c-ctmmeshconverg.htm

[28] Morlier, P. (2005) Creep in Timber Structure. CRC Press.

[29] Basuki, A., Awaludin, A., Suhendro, B. and Siswosukarto, S. (2018) Predicting Bending Creep of Laminated Veneer Lumber (LVL) Sengon (*Paraserianthes falcataria*) Beams from Initial Creep Test Data. *MATEC Web of Conferences*, **195**, Article ID: 02028

[30] O'Ceallaigh, C., Sikora, K., McPolin, D. and Harte, A.M. (2018) An Investigation of the Viscoelastic Creep Behaviour of Basalt Fibre Reinforced Timber Elements, *Construction and Building Materials*, **187**, 220-230. https://doi.org/10.1016/j.conbuildmat.2018.07.193

[31] Huang, Y. (2016) Creep Behavior of Wood under Cyclic Moisture Changes: Interaction between Load Effect and Moisture Effect. *Journal of Wood Science*, **62**, 392-399. https://doi.org/10.1007/s10086-016-1565-4

[32] Van De Kuilen, J.W.G. (2008) Creep of Timber Joints. *Heron*, **53**, 133-156.

[33] Laufenberg, T.L., Palka, L.C. and Mcnatt, J.D. (1999) Creep and Creep-Rupture Behavior of Wood-Based Structural Panels. U.S. Department of Agriculture, Forest Service, Forest Prod Lab, Madison.

[34] Holzer, S., Loferski, J. and Dillard, D. (1989) A Review of Creep in Wood: Concepts Relevant to Develop Long-Term Behavior Predictions for Wood Structures. *Wood and Fiber Science*, **21**, 376-392.

[35] Badan Standardisasi Nasional (National Standardiation Agency of Indonesia) (2013) SNI 1727: 2013 Beban minimum untuk perancangan bangunan gedung dan struktur lain (Minimum Load for Buildings and Other Structures Design).

[36] Badan Standardisasi Nasional (National Standardiation Agency of Indonesia) (2002) Tata Cara Perhitungan Struktur Beton Untuk Bangunan Gedung (Procedure of Concrete Structures Calculation for Buildings). SNI 03-2847-2002.

[37] Aicher, S., Reinhardt, H.W. and Garrecht, H. (2014) Materials and Joints in Timber Structures: Recent Developments of Technology. Springer, Dordrecht. https://doi.org/10.1007/978-94-007-7811-5

[38] Muñoz, W., Mohammad, M., Selenikovich, A. and Quenneville, P. (2008) Determination of Yield Point and Ductility of Timber Assemblies: In Search of Harmonised Approach. 10*th World Conference on Timber Engineering*, Miyazaki, 2-5 June 2008, 1064-1071.